UNIVERSITÀ DEGLI STUDI DI TORINO

Stefano Livraghi,Manuela Rolando,Sara Maurelli,Mario Chiesa,Maria Cristina Paganini,Elio Giamello
Nature of Reduced States in Titanium Dioxide as Monitored by Electron Paramagnetic Resonance. II: Rutile and Brookite Cases
JOURNAL OF PHYSICAL CHEMISTRY. C, NANOMATERIALS AND INTERFACES (2014) 118
DOI: 10.1021/jp5070374

On the Nature of Reduced States in Titanium Dioxide as Monitored by Electron Paramagnetic Resonance. II: the Rutile and Brookite cases.

Stefano Livraghi, Manuela Rolando, Sara Maurelli, Mario Chiesa, Maria Cristina Paganini, Elio Giamello*.

Dipartimento di Chimica, Università di Torino and NIS, Via P. Giuria 7, I - 10125 Torino, Italy

Abstract.

We have systematically used Electron Paramagnetic Resonance (EPR) to understand the nature of excess electron centers in Titanium dioxide and to classify their spectroscopic features. Excess electrons in TiO_2 (probably the most important photoactive oxide) have been generated either by photoinduced charge separation or by reductive treatments and are stabilized in the solid by titanium ions which reduce to paramagnetic Ti^{3+}. These are monitored by EPR and classified on the basis of their **g** tensor values in order to amend a certain confusion present in the literature about this subject. In the previous paper of this series (S. Livraghi et al. J. Phys. Chem. C 2011, 115, 25413) excess electron centers in anatase were investigated while the present one is devoted to rutile and brookite, the two other TiO_2 polymorphs, in the aim of providing a thorough and consistent guideline to researchers working in the wide area of titanium dioxide applications.

1. **Introduction**

Titanium dioxide is one of the most investigated metal oxides as it is a strategic material for both conventional usage (white pigment in paintings, paper, plastics etc.) and advanced applications such as photocatalysis,[1] water photosplitting,[2] dye-sensitized solar cells[3] (DSSC) and superhydrophylic coatings.[4] The essential step of all photochemical applications is the charge spatial separation which follows the irradiation of a crystal with photons of suitable energy. This entail the promotion of electrons (e^-) in conduction band (CB) and the formation of holes (h^+) in the valence band (VB).[5]

$$TiO_2 + h\nu \rightarrow e^-_{(CB)} + h^+_{(VB)} \qquad (1)$$

The light induced separation is followed by migration of the carriers to the surface, charge trapping and, eventually, charge transfer to adsorbed entities.[6,7] The primary electron traps in titania are Ti^{4+} ions which, upon trapping, formally reduce to Ti^{3+}. It is therefore understandable that nature, location and features of the charge traps in this solid are all issues of vital importance.

Titanium dioxide is also a reducible oxide as it loses O_2 from the lattice when the oxygen partial pressure in the atmosphere over the solid is decreased even at moderate temperatures. This causes the simultaneous formation of oxygen vacancies and excess electrons into the reduced solid according to the following equation:

$$O^{2-} + 2Ti^{4+} \rightarrow \tfrac{1}{2}\, O_2 + V_O^{\cdot\cdot} + 2\, Ti^{3+} \qquad (2)$$

where the oxygen vacancy is indicated using the Kröger and Vink notation and is usually thought to be empty as excess electrons are stabilized under the form of paramagnetic Ti^{3+} ions. Due to the prominence of titanium dioxide and to the many open problems concerning this matrix, it is not surprising that TiO_2 has been the subject of many experimental [8,9,10] and computational investigations [11,12] aimed at clarifying the structure of the surface, the phenomena of charge transport [13,14] and of charge stabilization.[15,16,17]

The two most important polymorphs of titanium dioxide are rutile and anatase. A third, less known polymorph is brookite. In spite of the fact that anatase and P25 (a solid prepared by oxidation of metallic titanium and containing both rutile and anatase partially connected by a specific interface) are the most interesting TiO_2 phases under the point of view of the photochemical applications, rutile, the most stable thermodynamic phase, has been much more investigated by surface scientists due to the fact that growing single crystals or single crystalline layers of this polymorph is easier. The oxygen loss and the behaviour of anion vacancies and reduced centres upon reoxidation, in fact, have been studied in detail mostly in the case of single crystals[18,19] and, at a lesser extent due to the complexity of the system, in the case of powdered materials. We are thus facing the

paradox of a great deal of basic research available on rutile and a parallel intense activity in applied research on anatase and P25. As far as the brookite polymorph is concerned, a relatively smaller number of studies is available even though, in the last years, the number of papers related to this material has rapidly grown [20,21,22].

The present paper is the second of a short series aimed at rationalizing the features of excess electron centres in titanium dioxide exploiting the potential of the Electron Paramagnetic Resonance (EPR) technique. In the first paper of this series [23] we reported the EPR spectra of excess electron centres in nanocrystalline anatase while the present one is devoted to rutile and brookite polymorphs. The use of EPR investigation of reduced states of titanium dioxide appears as a natural choice due to the high potential of the technique in describing paramagnetic defects in solids.[24] However, despite a relatively high number of papers devoted to EPR of reduced centres in TiO_2, a clear-cut picture of the electron stabilizing sites in the various polymorphs of this strategic solid is not yet available. The present paper, together with the previous one,[23] is an effort to fill this gap.

2. Experimental.

In this work, three different TiO_2 polymorphs were used. Commercial micro-rutile (hereafter μ-rutile) from Sigma Aldrich (Saint Louis, MO, USA) containing about 5% of anatase with a surface area of ca. 2 m^2/g.[25]

The second one was the commercial Aeroxide P25 from Evonik (Essen, Germany), which is considered a benchmark in the fields of photocatalysis and photovoltaics owing to its high activity (here after P25). P25 is prepared by flame pyrolysis of $TiCl_4$ and contains a mixture of about 75 – 85% anatase and 15 – 20% rutile, but also some amorphous part.[26] The P25 surface area is ca. 50 m^2/g.

Brookite samples were kindly provided by Prof. L. Palmisano (University of Palermo) and prepared via thermohydrolysis of $TiCl_4$. The brookite surface area is c.a. 70 m^2/g.[27,28]

Activation of TiO_2 samples were carried out according to the following standard procedure: first, outgassing under high vacuum (residual pressure < 10^{-4} mbar) at 673 K for 0.5 hours in order to remove adsorbed water and other surface impurities. Since the vacuum treatments cause oxygen loss from the solid, a successive treatment under 20 mbar O_2 at the same temperature was performed to recover a fully oxidized state. In some cases, for the sake of comparison and in order to investigate systems similar to those employed in photocatalysis, experiments were carried out on materials simply outgassed at room temperature, and therefore containing surface contaminants such as chemisorbed water or surface hydroxyl groups.

X-band Continuous Wave (CW) EPR spectra have been recorded on a Brucker EMX spectrometer equipped with a cylindrical cavity and operating at a 100 kHz field modulation. The measurements were carried out at the liquid nitrogen temperature (77 K) in quartz cells that can be connected to a conventional high-vacuum apparatus (residual pressure < 10^{-4} mbar). EPR spectra were simulated using the Easyspin package.[29]

XRD spectra were collected on a difractometer (PW1830, Phillips) using Co (Kα) radiation. Diffraction patterns were refined with Rietveld method using the MAUD (Material Analysis Using Diffraction) program.[30]

3. Results and discussion.

3.1. X-ray diffraction of the investigated materials

The XRD patterns of the two kinds of TiO_2 samples adopted in this work are shown in Fig.1. In commercial μ-rutile a small contamination due to anatase (~5%) is observed. In the case of brookite, the best fit of the diffraction pattern was achieved uniquely considering the data corresponding to this polymorph. The commercial μ-rutile sample, constituted by relatively large crystals, shows sharp diffraction peaks with respect to those of the nanocrystalline brookite (Table 1). It is worth noting that, despite the excellent match of the experimental XRD pattern and the fit in Fig.1, the relatively large width of the diffraction peaks of brookite together with the correspondence of few of them with peaks typical of anatase could mask a relatively small contamination (if any) due to the latter polymorph.

Sample	Phase composition	wt %	Crystallite Size (nm)	Rw (%)
μ–rutile (ex-Aldrich)	rutile	95	~1000	11
	anatase	5	~500	
brookite	brookite	100	~30	4.8

Table 1. Rietveld refinement on the XRD patterns of μ-rutile and brookite polimorphs.

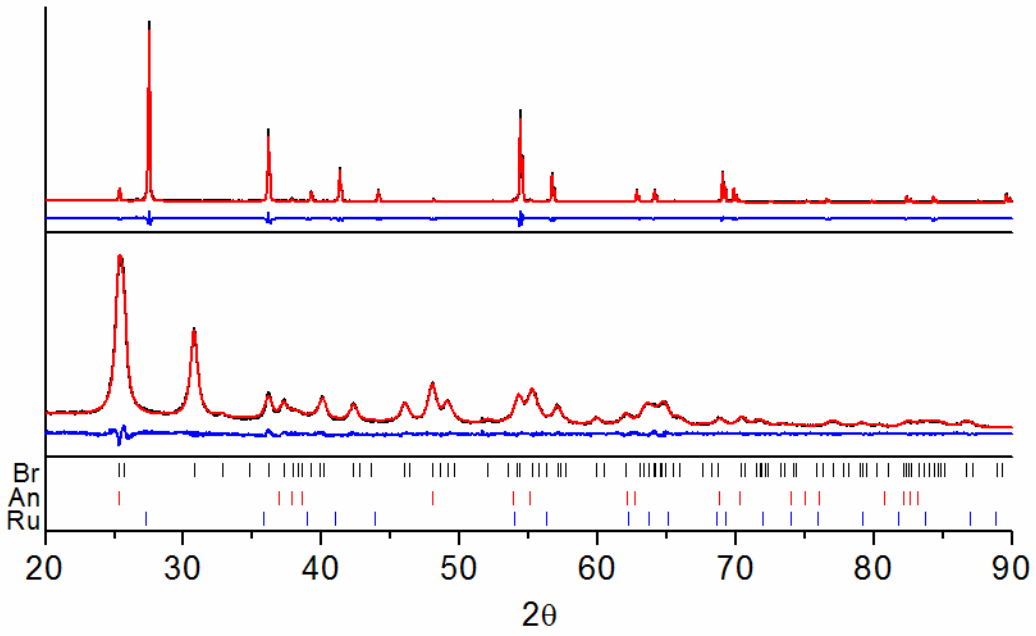

Figure 1. XRD patterns of μ–rutile (top) and brookite (bottom). Black line: experimental trace. Red line: computer simulation obtained by Rietveld refinement. Blue line: difference between experimental e simulated patterns. In the bottom of the figure the peaks position for brookite (Br), anatase (An) and rutile (Ru) are reported.

3.2 Electron trapping in μ-rutile.

In the previous paper of this series[23] we were able to unambiguously assign the EPR features of Ti^{3+} centers corresponding to the regular lattice positions in the bulk of anatase crystals. This was done using a material doped with an aliovalent element bearing an extra electron (F and/or Nb).[31,32] The same convenient approach could not be extended to rutile since the extra electron carried by Nb, in Nb-doped rutile, is not transferred to Ti ions.[33,34] We tried also to obtain F-doped rutile by high temperature treatments of doped anatase. In this case, however, the solid loses practically all the dopant during the phase transformation and bare rutile was eventually obtained. To investigate Ti^{3+} centres in rutile we have therefore to rely exclusively on irradiation-induced charge separation, and on materials where excess electrons are generated either by annealing under vacuum or by chemical treatments.

3.2.1 μ-rutile reduction via annealing under vacuum and oxygen depletion.

Fig. 2 reports the CW-EPR spectra recorded after a progressive, stepwise, thermal annealing of μ-rutile in the temperature range 373 – 673K.

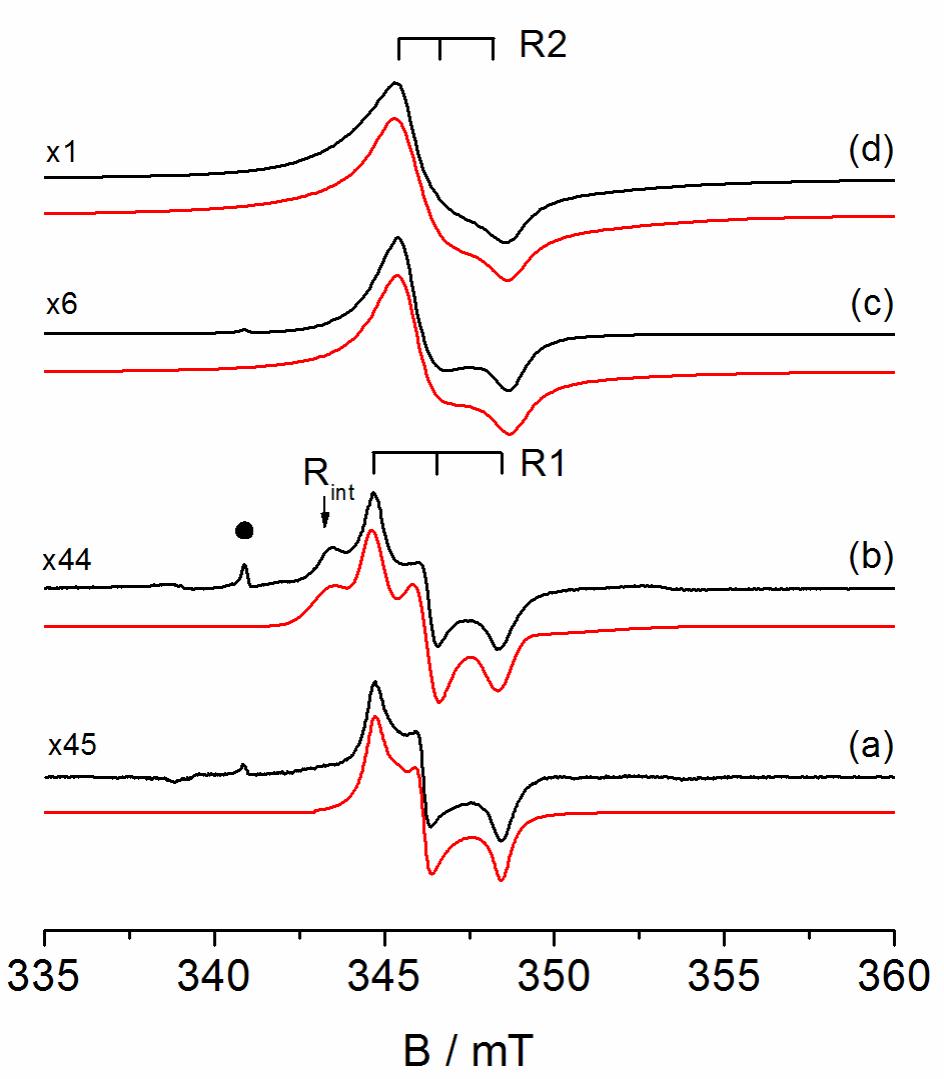

Figure 2, Experimental (black lines) and computer simulations (red lines) X-band CW EPR spectra of μ-rutile run at 77K after thermal annealing in vacuum at different temperatures: (a) 45 minutes at 373K, (b) 45 minutes at 473K, (c) 45 minutes at 473K after step (b), 45 minutes at 773K. The EPR intensities are normalized to the spectral intensity of spectrum (d). The series of numerical factor on the left measure the various intensity ratios. The dot indicates traces of Ti^{3+} in the anatase impurity.

No EPR signal was observed in the starting material, as expected for fully stoichiometric TiO_2. The early steps of reduction (Fig. 2 (a) and (b)) up to T = 473K cause the appearance of weak and relatively sharp EPR spectra due to the overlap of two akin signals whose **g** tensor structures were derived by computer simulation (red lines in Fig. 2 and Table 2). Both signals show a **g** tensor typical of Ti^{3+} species in a distorted octahedral environment. The weaker species is characterized by the *g* values g_1=1.978, g_2=1.975, g_3=1.942 coinciding with those of the interstitial Ti^{3+} centers assigned by Hasiguti [35] and Hajimoto [36] in a single crystal of rutile and observed, more recently, by some of us in a polycrystalline system of non stoichiometric "blue" rutile[37] prepared via hydrolysis of $TiCl_4$. This signal is labeled as $R_{int,}$ where R stands for rutile. The second, more intense signal (hereafter R1) also has an orthorhombic symmetry ($g_1 \neq g_2 \neq g_3$) with *g* values g_1 =

1.970, g_2 = 1.961, g_3 = 1.948 (a stick diagram in Fig. 2). More prolonged thermal treatments (Fig. 2, (c) and (d)) cause a net and progressive intensity increase of the EPR spectra, which become dominated by a new rhombic Ti^{3+} signal (hereafter R2) characterized by g_1=1.966, g_2=1.961 and g_3=1.948 (Table 2) and slightly broader than the previous ones. The difference between the **g** tensors of R1 and R2 is limited to a small variation of g_1 (0.004).

Summarizing, as already observed for the anatase polymorph, proceeding from mild reduction conditions to higher reduction temperatures different EPR signals amenable to Ti^{3+} are detected. However, at variance with the case of anatase, the differences between the spin-Hamiltonian parameters of signals R_{int}, R1 and R2 are rather small. Furthermore, both R1 and R_{int} are formed at the very beginning of the reduction process (annealing at low temperatures) and play a minor role in quantitative terms when the treatment is performed at higher temperatures. In such a case (higher degree of reduction) the R2 species is the dominant one and represents the fundamental electron trapping site of μ-rutile reduced by thermal annealing with generation of oxygen vacancies.

3.2.2. Electrons injection in μ-rutile via atomic hydrogen.

An alternative way to generate excess electrons in titanium dioxide is represented by UV light irradiation in a hydrogen atmosphere at 77K. In this case, UV photons induce charge separation and the photo-formed hole, once migrated to the surface, reacts with molecular hydrogen (homolytic splitting) to give an hydroxyl group and an H atom which, in turn, ionizes injecting an electron in the solid.[38]

$$h^+ + O^{2-}_{(surf)} \rightarrow O^-_{(surf)} \qquad (3)$$

$$O^-_{(surf)} + H_2 \rightarrow OH^-_{(surf)} + H^\cdot \qquad (4)$$

$$H^\cdot + Ti^{4+}\text{-}O^{2-}_{(surf)} \qquad Ti^{3+} + OH^-_{(surf)} \qquad (5)$$

Figure 3 compares the EPR spectrum of μ–rutile obtained upon the described procedure (equations 3-5, Fig. 3(b)) with that recorded after the mild thermal annealing at 373K (Fig.s 2(a) and 3(a)). Apart from the intensity (much higher in the case of spectrum 3b) and from small differences in the line width, the spectra reported in Fig. 3 are basically coincident and amenable to the sole contribution of the same rhombic species already described in the previous paragraph and labelled R1 (Table 2). The higher intensity of spectrum 3b confirms the efficiency of the UV-H_2 method in injecting extra electrons into the solid.

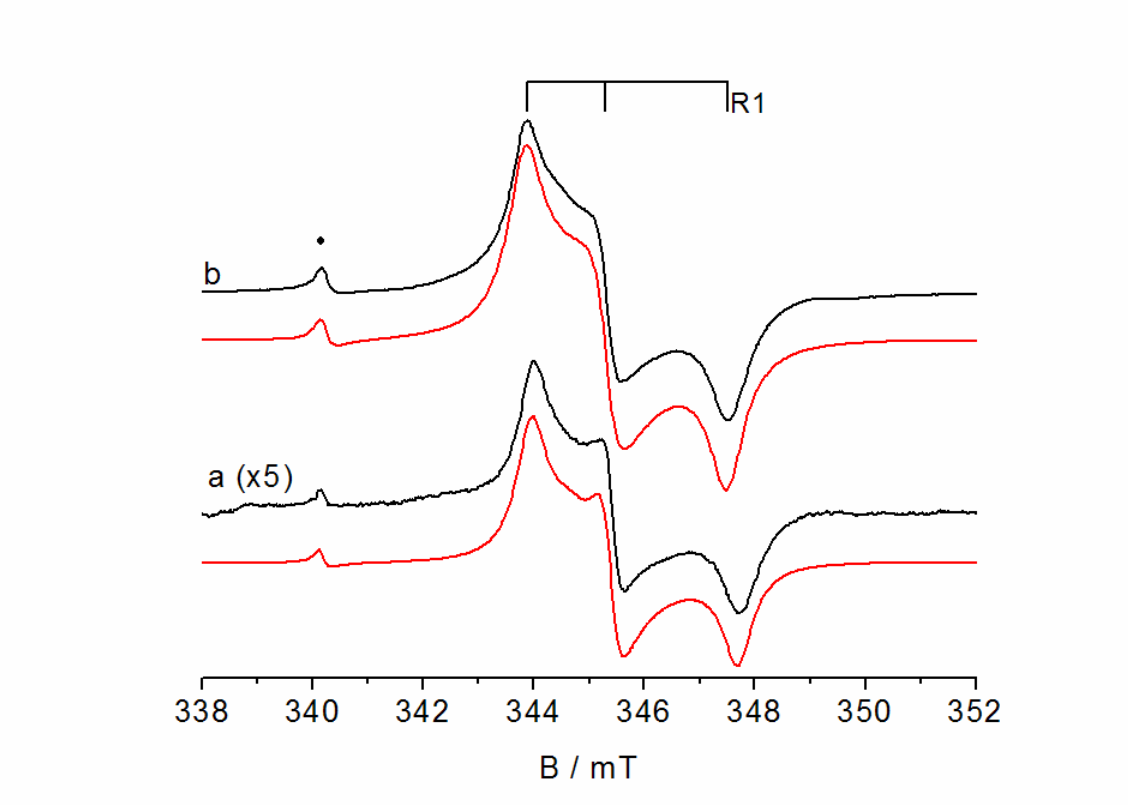

Figure 3. Experimental (black line) and computer simulated (red line) CW-EPR spectra of Ti^{3+} in μ-rutile recorded at 77K and obtained via: (a) annealing under vacuum at 373 K for 45min; (b) UV irradiation in H_2 atmosphere at 77K.

3.2.3. Electron trapping in μ-rutile upon photo-induced charge separation

The observation of the electron trapping sites upon photo-induced electron-hole separation performed under vacuum is partially hampered by the fast charge carrier recombination in such conditions [39]. Fig. 4 reports the EPR spectra observed after irradiation under vacuum at 77K of μ–rutile in two distinct conditions. Figure 4(b) concerns an activated fully dehydrated sample (standard treatment described in Section 2). Though rather weak, an EPR signal amenable to Ti^{3+} and corresponding to the R2 center is observed. At lower magnetic field the typical signal of an hole (O^-) in TiO_2 also appears. Both signals disappear after warming the sample at RT due to recombination of the charge carriers. A minor feature constituted by a weak shoulder at g ~ 1.977 is the trace of the interstitial Ti^{3+} center (R_{int}) previously described.[35,36,37]

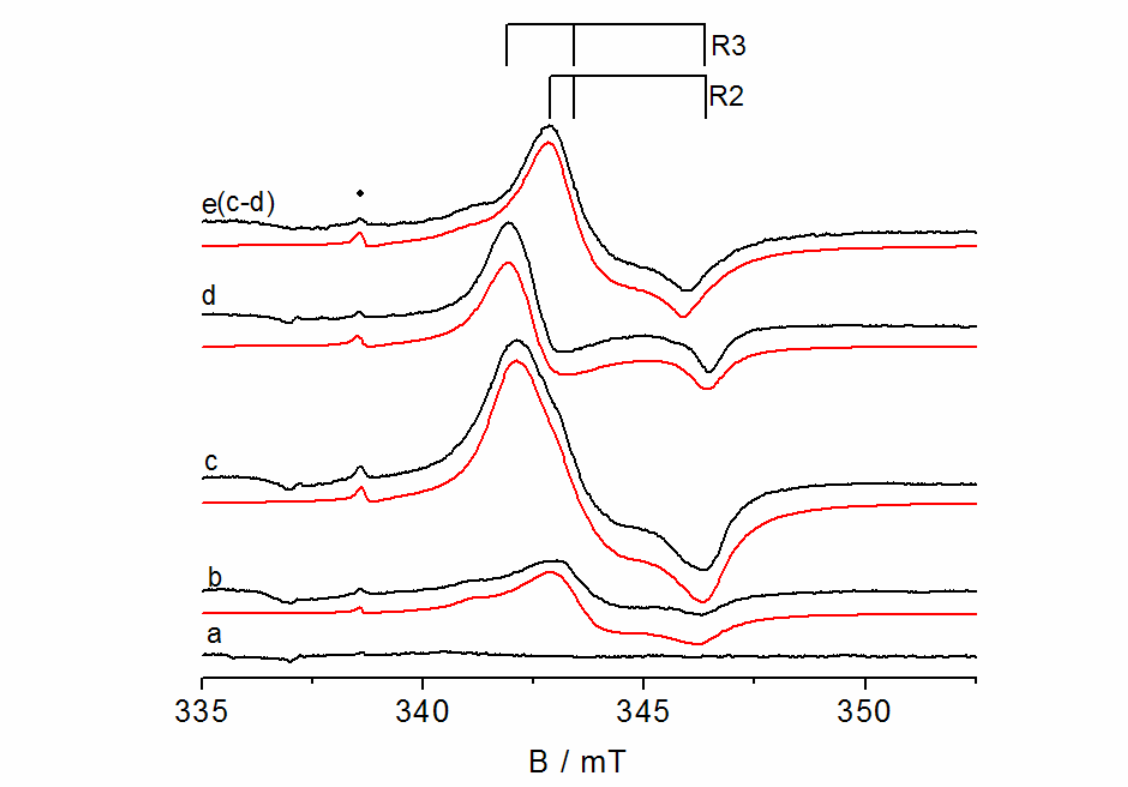

Figure 4. Experimental (black lines) and computer simulations (red lines) CW-EPR spectra recorded after irradiation of μ-rutile at T = 77K. (a) background, (b) after UV irradiation under vacuum, (c) after UV irradiation in the presence of adsorbed water, (d) after warming the same sample at RT for few seconds and successive cooling. Spectrum (e) is the (c)-(d) difference. The spectra are all recorded at T = 77K.

Previous investigations of the charge separation processes in titania, performed in aqueous suspensions of the solid, showed EPR spectra characterized by higher intensity than that observed upon irradiation in vacuum.[40] For this reason we also performed the UV irradiation on a sample rehydrated, after the initial standard activation (Section 2) by adsorption of 5mbar water vapor at RT. In such conditions both surface OH^- groups and adsorbed molecular water are formed. The spectrum obtained by irradiation of such a sample is shown in Fig. 4(c) and is characterized by a more intense and more complex Ti^{3+} signal with respect to that in Fig. 4(b). This difference is likely due to the reactivity of a fraction of the photogenerated holes either with surface water or OH^- groups so that these centers cannot recombine with the electrons associated to Ti^{3+} ions. The spectrum in Fig 4(c) is given by the overlap of two rhombic Ti^{3+}species (computer simulation in Fig. 5, panel A), namely the already described R2 species and a new species (hereafter R3) whose *g* values are, once again, very similar to those of R1. Heating the sample at RT for few seconds causes a modification of the signal in Fig.4(c) which loose intensity due to further e^- - h^+ recombination. This process is selective and involves exclusively R2 centers leaving unaffected species R3 whose signal shows up after warming and recombination (Fig.4(d)). Correspondingly the profile of the more labile R2 species appears if one subtracts spectrum 4(d) from spectrum 4(c)

(Fig.4(e)). The described UV irradiation of hydrated samples shows therefore the appearance of a Ti^{3+} species not observed in the case of fully dehydrated materials, whatever the generation method. This evidence suggests a crucial role of adsorbed water and/or of surface OH^- groups in the stabilization of R3 species. The interpretation is confirmed by the result of the irradiation of an as prepared, untreated sample simply outgassed at RT (in these conditions both surface OH^- groups and chemisorbed molecular water are present at the surface[41]) which essentially shows the same features of spectrum in Fig. 4(c). The EPR spectra of the two irradiated samples (activated-rehydrated and as prepared) are compared in Fig. 5 (Panels A and B, respectively) which shows by computer simulation that both spectra are determined by the presence of similar fractions of R2 and R3 centers.

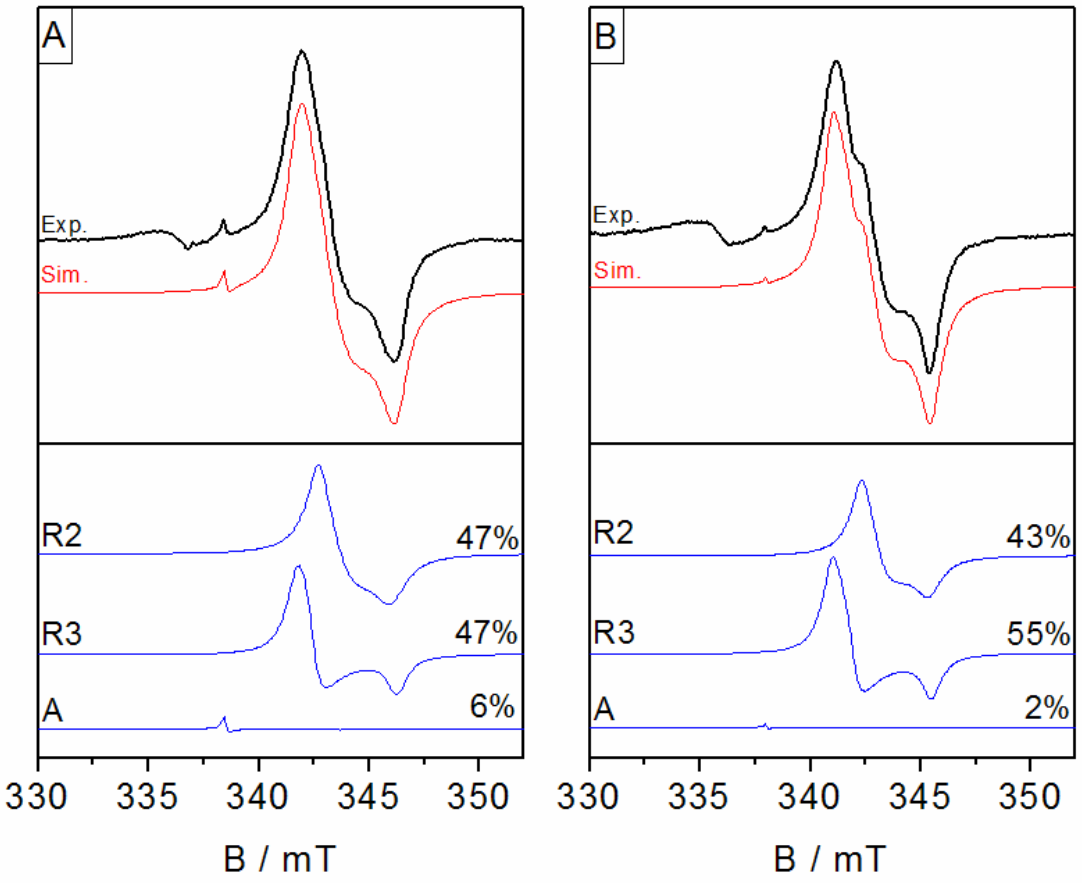

Figure 5. Experimental and computer simulated (red lines) CW-EPR spectra recorded at 77K of UV irradiated μ-rutile. Panel A: spectrum obtained with an activated sample after H_2O absorption (see Fig. 4c). Panel B, spectrum obtained irradiating a non activated sample simply outgassed at RT. The lower panels show the distinct species (R2, R3 and A) contributing to the simulations with the corresponding abundances.

On the basis of the similarities between the spectral parameters of R1 and R3 it seems reasonable to hypothesize that R3 results from the modification of R1 by the effect of the interaction with surface adsorbed OH^- groups and H_2O molecules. To get a deeper insight into this issue an analysis of the

interaction of the Ti^{3+} centers with the surrounding nuclei could be decisive. However, our efforts to use highly sensitive pulse EPR techniques to investigate the interactions of R1, R2 and R3 with the surrounding magnetically active nuclei (surface protons, ^{17}O ions introduced in the solid) were unsuccessful as, for highly reduced samples (thermal treatments at high temperatures) no electron spin-echo could be detected because of the fast relaxation time T_M, while for the mildly reduced system, showing the only R1species in the field swept spectrum, the echo recorded at T = 6K (see SI) was too weak and no nuclear modulations could be observed.

3.2.4 *Ti^{3+} centers in μ-rutile: the assignement.*

The *g* values of the distinct EPR signals (R1-R3 and $R_{int.}$) due to Ti^{3+} ions in variously treated μ-rutile samples are summarized in Table 2. The signals are found in the same spectral region and are characterized by a modest degree of rhombicity ($g_1 \neq g_2 \neq g_3$). The formation of each species is strictly related to the procedure to generate excess electrons in the solid. In the following the features and a possible assignment of each species in μ-rutile is discussed.

The *g* values corresponding to the signal labelled R_{int} are close to those reported for interstitial Ti^{3+} in rutile single crystals annealed at high temperature. [35,36] By the way, the geometry of the interstitial sites is not so different from that of the regular lattice one. In the present sample the concentration of interstitial sites upon annealing (Fig. 2) is however extremely low and these sites actually have a marginal role in the electron trapping processes taking place in rutile. To ascertain whether interstitial Ti^{4+} ions pre-exist to their reduction by various treatments (Frankel defects) or are formed upon a structural rearrangement due to the oxygen loss, is therefore not important.

The main signals observed in rutile (R1-R3) have in common two of the three g tensor elements. This firmly suggests that we are dealing with Ti^{3+} centers differing for relatively minor structural features. Among all signals here reported R1 shows the highest rhombic character and is observed when excess electrons are generated in mild conditions (*i.e.* thermal annealing at $T \leq 473K$ or via electron injection from the surface) while it is not observed when electrons are associated to charge carrier separation induced via UV light absorption. The R1 center can tentatively be identified with Ti^{3+} centers at the surface or near the surface of the microcrystals. Considerations about R2 and R3 in the following will corroborate this interpretation.

Thermal annealing experiments have shown that R2 centres are associated to excess electrons in partially reduced systems. In fact the R2 EPR signal appears at $T \geq 473K$ and becomes by far the dominant one at higher reduction temperatures (Fig.2). R2 signal can be assigned to Ti^{3+} centers at the regular (*i.e.* non interstitial) cationic sites of the rutile structure for a series of reasons here reported. First of all the μ-rutile sample employed in the present study has a very low specific

surface area (about 2 m^2/g) and quite large crystals if compared with typical nanostructured solids. In our case, therefore, the fraction of bulk ions is largely dominant with respect to that of surface ions (a rough estimate indicates that surface ions are only 0.01% of the total). It is consequently more than reasonable to connect the reduced centers formed in high amount by progressive annealing (and oxygen depletion) of the solid with the bulk of the crystal. The high temperature of the annealing treatment should allow the migration (by hopping) of the trapped electrons towards the bulk even if they are generated by depletion of oxygen from surface or subsurface regions. The only alternative one should, in principle, consider for R2 is that of a Ti^{3+} bulk ion located nearby an oxygen vacancy. This second case however can be definitely excluded as the *g* values of such a site have been monitored in a irradiated rutile single crystal studied by Halliburton and co-workers [42] and are, as expected because of the relatively low symmetry, much more rhombic than all the signals reported in the present work (g_1=1.9572, g_2=1.9187, g_3=1.8239). A second fundamental consideration is that R2 also forms upon UV irradiation of the solid at low T (Fig. 4 (b), (c), (e)) in the absence of oxygen vacancies.

Finally, the R3 center, which is observed exclusively in the case of hydrated materials (Fig. 4 and 5) can be interpreted as a modification of R1 due to the interaction of the latter with surface hydoxyls. R1 in fact, which is observed after contact of atomic H with the surface does not appear at all in the spectra corresponding to an hydrated surface. This observation strengthens the assignment to a surface center proposed before for R1.

3.4 *Electron trapping in brookite.*

Brookite is relatively less studied in comparison with the more common anatase and rutile since a brookite phase free from contamination of the other two polymorphs is rather difficult to prepare. Notwithstanding, since in the last few years the interest for brookite has rapidly grown and the preparation methods improved [27], the lack of data on excess electron centres in this material prompted us to investigate this polymorph. Like anatase and rutile also brookite's structure is based on distorted TiO_6 octahedra with tri-coordinated oxygen ions (OTi_3). Each TiO_6 unit shares three edges with nearby octahedral producing an orthorhombic structure.

The EPR spectra resulting from from electron injection (eq. 3-5) and from charge separation upon UV irradiation (eq. 1) both performed on material simply outgassed at room temperature are reported in Fig. 6a and 6b respectively. These EPR spectra bear a closer resemblance with those observed for anatase rather than with those of μ-rutile. Two distinct signals are identified in the region of Ti^{3+} species, namely a narrow axial Ti^{3+} signal (species B1) with components at $g_{\|}$=1.960 and $g_{\perp}$= 1.989 and a broad apparently symmetric signal centred at about g = 1.93 (B2).

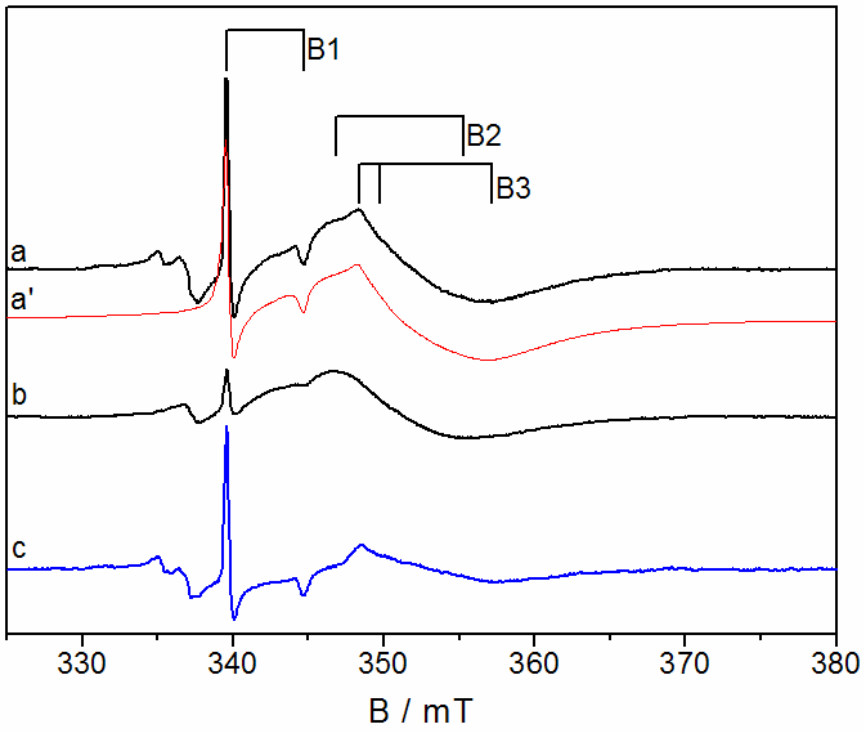

Figure 6. Experimental CW-EPR spectra of UV-irradiated brookite: (a) at 77K in H_2 atmosphere, (b) at 77K under vacuum; (c) spectrum obtained subtracting (b) from (a). Spectrum (a') is the computer simulation of spectrum (a), (spin-Hamiltonian parameters in Table 2).

Electron injection via irradiation under H_2 (Fig. 6a, computer simulation in a') leads, also in this case, to a more intense spectrum than that obtained by simple irradiation under vacuum (6b), however the regular line shape of species B2 is partially perturbed by the superimposition of a third Ti^{3+} species (B3) that can be put into evidence by subtracting the spectroscopic features of spectrum (b) from those of (a) (Fig. 6c). The simulation (6a'), corroborated by data obtained using a second batch of brookite and reported as S.I., show that this third signal is characterized by a rhombic **g** tensor (g_1=1.939, g_2= 1.929 and g_3=1.893). The relative abundance of the axial signal B1 amounts to 3.4% of the overall spectral intensity, the others being 93.2% (B2) and 3.4% (B3).

The **g** tensor elements corresponding to the described signals are summarized in Table 2. B2 and B3 lie in the same magnetic field region and it is reasonable to suppose that they do not belong to structurally distinct species. Signal B2 could in fact be due to species of the B3 family in reciprocal dipolar interaction in a region of the crystal where their concentration is high. In analogy with what demonstrated in the case of anatase (wide, poorly structured signals at relatively high field) we suggest that also in the present case the Ti^{3+} ions giving origin to the broad B2 and B3 signals at a

relatively high magnetic field are located in the disordered region at the surface of the perturbed nanocrystals. The presence of various crystal faces, of morphological defects and the perturbation corresponding to the presence of surface hydroxyl groups (eq. 5) fully explain the local disorder occurring at the surface and ending up in a substantial *g* strain. The same does not occur in the case of μ-rutile (Section3.2) since the low surface area of the material severely limits the role of the surface.

Signal B1 observed for brookite deserves a particular comment as there is a strong resemblance between the features of this axial and narrow signal and those of signal A1 (corresponding to the regular lattice position in the bulk of anatase[23,43]). The presence of a fraction of anatase in the prepared brookite is not completely excluded (see Section 3.1) however signal B1 seems to be too intense to be related to electron trapped in an impurity of the solid. Moreover the *g* values of A1 and B1 are similar but not exactly coincident. B1 therefore is assigned to an excess electron center in the bulk of brookite which shows an electron trapping behaviour parallel and quite similar to that shown by anatase and described in previous papers.

Polymorph	Center	g_1	g_2	g_3	Main features	Ref.
Rutile	$R_{int.}$	1.978	1.975	1.942	Interstitial site	This work, 35,36,37
	R1	1.970	1.961	1.948	Surface or subsurface site (dehydrated surface)	This work
	R2	1.966	1.961	1.948	Bulk lattice site	This work
	R3	1.973	1.961	1.948	Surface or subsurface site (hydrated surface)	This work
Brookite	B1	$g_\perp$= 1.989		$g_\parallel$=1.960	Bulk lattice site.	This work
	B2, B3	g_{av} = 1.93			Surface Ti^{3+} sites, broad signal because of surface heterogeneity	This work
		1.939	1.929	1.893		
Anatase	A1	$g_\perp$= 1.992		$g_\parallel$=1.962	Bulk lattice site. Delocalized electron	23,43
	A2	g_{av} = 1.93			Surface Ti^{3+} sites, broad signal because of surface heterogeneity	23,43

Table 2. Synopsis of the **g** tensors of Ti^{3+} centres monitored by EPR in the three polymorphs of titanium dioxide (A= Anatase, B = Brookite, R = Rutile).

3.5 *Conclusive remarks: electron localisation and site symmetry.*

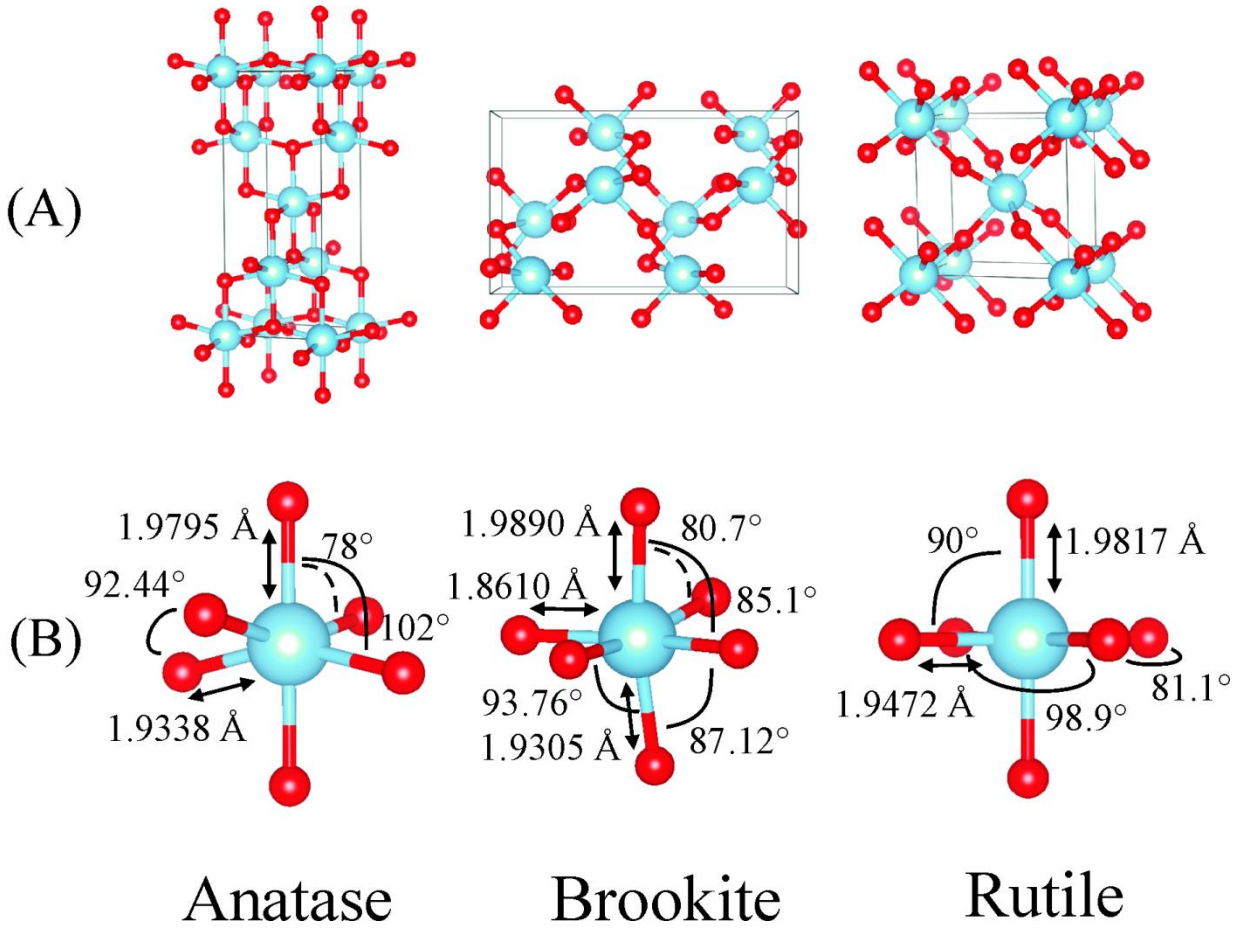

Scheme 1. Crystal structure of the three polymorphs of TiO_2, namely anatase, brookite and rutile. Blue and red spheres stand for Ti and O atoms, respectively. The unit cell of the three structures is reported in (A), while in (B) an enlargement of the local ligand coordination around the Ti atoms for the three polymorphs is shown. The structures are rearranged from Ref.[44,45]

The CW-EPR analysis of trapped electron centers (Ti^{3+}) in μ-rutile and brookite performed in the present work allowed us to accomplish a picture of the EPR features of such centres for all the polymorphs of titanium dioxide, whose crystal structures are reported in Scheme 1A. This analysis started with the EPR investigation of anatase [23], followed by the study on the properties of the interstitial Ti^{3+} in rutile.[37] For these two systems the favourable relaxation times of the reduced species allowed us to monitor the spin delocalisation over the oxygen ions surrounding the Ti centres using hyperfine spectroscopy. In the case of interstitial centers in rutile the result is similar to that of molecular Ti^{3+} compounds[46] with a full localisation of the unpaired electron wave function in the *d* orbitals of the metal ions. As opposite, for the A1 center in anatase we found a result compatible with an extended delocalisation of the spin.

From the rutile spectra here reported, two different sites are distinguished, namely R2 at bulk lattice sites and R1-R3 reasonably located near the clean (R1) or hydrated (R3) surface. All signals

observed in rutile have a slightly distorted octahedral symmetry ($g_1 \neq g_2 \neq g_3$) with a very modest degree of rhombicity similar to that found for interstitial species (R_{int}) and in agreement with the symmetry of the cationic site of the crystal structure, shown in Scheme1B. It is worth noting that these structures are derived from X-ray diffraction of stoichiometric undefective oxides and that it is impossible to consider in our scheme the polaronic distortion induced by the presence of an excess electron (Ti^{3+}). At variance with our previous studies, in the case of the reduced rutile polymorph, the hyperfine techniques didn't allow to determine the unpaired electron wave function distribution. It is however quite likely that the full localisation of the spin in Ti *d*-orbitals (unambiguously demonstrated in the case of R_{int}) applies also in the case of the other R signals (R1, R2, R3) which have similar structure and g values.

As far as brookite is concerned we notice a close similarity between the EPR features of this polymorph (here reported for the first time) and those of anatase. In particular the **g** tensors of both A1 (lattice site in anatase) and B1 centers show axial symmetry. Considering the high level of distortion of the octahedral symmetry for the TiO_6 units in brookite (Scheme 1 B), the axial nature of the **g** tensor for this species is very likely due to the delocalized nature of the excess electron wave function, as already demonstrated for anatase [23], which produces a different, more symmetric, arrangement of the electron spin density. This point is currently under investigation in our laboratory.

In conclusion, this paper completes our previous study on the features of trapped electron sites (Ti^{3+} centers) in the three polymorphs of TiO_2 by means of EPR techniques. The whole set of experimental data here reported (Table 2) should be considered as a useful guideline for researchers working in the field.

Acknowledgmets.

The Authors wish to thank Prof. Leonardo Palmisano (Università di Palermo) for having kindly provided the sample of Brookite and Prof. Fernando Camara Artigas (University of Torino) for his help about the crystal structure of this polymorph. This work has been supported by the Italian Ministry of University and Research, MIUR, through the "National Funding for Basic Research" (FIRB) with a project entitled "Oxides at the nanoscale: functionalities and applications" (FIRB RBAP11AYN). Thanks are also due to the COST Action CM1104 (Reducible oxides: chemistry, structure and functions).

References:

1 Fujishima, A.; Rao, T. N.; Tryk, D. A. Titanium Dioxide Photocatalysis. *J. Photochem. Photobiol C: Photochemistry Reviews* **2000**, 1, 1–21.
2 Honda, K.; Fujishima A. Electrochemical Photolysis of Water at a Semiconductor Electrode. *Nature* **1972**, *238*, 37-38.
3 Hagfelt, A.; Grätzel, M. Light-Induced Redox Reactions in Nanocrystalline Systems. *Chem. Rev*. **1995**, 95, 49-68.
4 Martra, G.; Anpo Verification of the Photoadsorption of H2O Molecules on TiO2 Semiconductor Surfaces by Vibrational Absorption Spectroscopy, *J. Phys. Chem. C* 2007, 111, 9811-9817.
5 Linsebigler, A.L; Lu, G.Q.; Yates, J. T. Photocatalysis on TiO_2 surfaces: Principles, Mechanisms, and Selected Results. *Chem. Rev*. **1995**, *95*, 735-758.
6 Chen, X.; Mao, S. S. Titanium Dioxide Nanomaterials: Synthesis, Properties, Modifications, and Applications. *Chem Rev.*, **2007**, 107, 2891-2959.
7 Chiesa, M.; Paganini, M.C.; Giamello, E. EPR of Charge Carriers Stabilized at the Surface of Metal Oxides. *Appl. Mag. Res.*, **2010**, 37, 605-618.
8 Diebold, U. The surface Science of Titanium Dioxide. *Surf. Sci. Rep*. **2003**, *48*, 53-229.
9 Henderson, M. A. A Surface Science Perspective on TiO_2 Photocatalysis. *Surf. Sci. Rep.* **2011**, 66, 185–297.
10 Macdonald, I. R.; Howe, R. F.; Zhang, X.; Zhou, W. In Situ EPR Studies of Electron Trapping in a Nanocrystalline Rutile. *J. Photochem. Photobiol. A* **2011**, 216, 238–243.
11 Morgan, B.J.; Watson, G.W. A DFT + U description of oxygen vacancies at the TiO_2 rutile (1 1 0) surface. *Surf. Sci.* **2007**, *601*, 5034-5041.
12 Gong, X-Q.; Selloni, A.; Batzill, M.; Diebold, U. Steps on anatase TiO2(101). *Nature Materials* **2006**, 5, 665-670.
13 Deskins, N.A.; Dupuis, M. Intrinsic Hole Migration Rates in TiO_2 From Density Functional Theory. *J. Phys. Chem. C* **2009**, 113, 346-358.
14 Deskins, N. A.; Rousseau, R.; Dupuis, M. Defining the Role of Excess Electrons in the Surface Chemistry of TiO_2. *J. Phys. Chem. C* **2010**, *114*, 5891-5897.
15 Di Valentin, C.; Pacchioni, G.; Selloni, A. Electronic Structure of Defect States in Hydroxylated and Reduced Rutile TiO_2(110) Surfaces. *Phys. Rev. Lett.* **2006**, *97*, 166803
16 Finazzi, E.; Di Valentin, C.; Pacchioni, G. Nature of Ti Interstitials in Reduced Bulk Anatase and Rutile TiO_2. *J. Phys. Chem. C* **2009**, *113*, 3382-3385
17 Di Valentin, C.; Pacchioni, G.; Selloni, A. Reduced and n-Type Doped TiO_2: Nature of Ti^{3+} Species. *J. Phys. Chem. C* **2009**, *113*, 20543-20552.
18 Li, M.; Hebenstreit, W.; Diebold, U. Oxygen-Induced Restructuring of the Rutile TiO_2 (110)(1 × 1) Surface. *Sur. Sci.* **1998**, 414, L951-L956.
19 Yim, C. M.; Pang, C. L.; Thornton, G. Oxygen Vacancy Origin of the Surface Band-Gap State of TiO_2(110)**.** *Phys. Rev. Lett.* **2010**, 104, 036806.
20 Pottier, A.; Chanéac, C.; Tronc, E. Mazerolles, L. Jolivet, J-P. Synthesis of Brookite TiO_2 Nanoparticles by Thermolysis of $TiCl_4$ in Strongly Acidic Aqueous Media. *J. Mater. Chem.* **2001**, 11, 1116–1121.
21 Di Paola, A.; Bellardita, M.; Marc, G.; Palmisano, L.: Parrino, F.; Amadelli, R. Preparation of Sm-loaded brookite TiO_2 photocatalysts. *Cat. Today* **2011**, 161, 35-40.
22 Ohno, T.; Higo, T.; Murakami, N.; Saito, H.; Zhang, Q.; Yang, Y.; Tsubota, T. Photocatalytic Reduction of CO_2 Over Exposed-Crystal-Face-Controlled TiO_2 Nanorod Having a Brookite Phase with co-Catalyst Loading. *Appl. Catal. B-Environ* **2014**, 152–153, 309–316.
23 Livraghi, S.; Chiesa, M.; Paganini, M.C.; Giamello, E. On the Nature of Reduced States in Titanium Dioxide as Monitored by Electron Paramagnetic Resonance. I: The Anatase case. *J. Phys. Chem.* **2011**, 115, 25413-25421.
24 Chiesa, M.; Giamello E. *"Electron Paramagnetic Resonance of Charge Carriers in Solids"* in M. Brustolon and E. Giamello Ed.s *Electron Paramagnetic Resonance: a practitioner's toolkit* Wiley 2010
25 Mino, L.; Spoto, G.; Bordiga, S.; Zecchina, A. Rutile Surface Properties Beyond the Single Crystal Approach: New Insights from the Experimental Investigation of Different Polycrystalline Samples and Periodic DFT Calculations. *J. Phys. Chem. C* **2013**, 117, 11186−11196.

26 Ohtani, B.; Prieto-Mahaney, O. O.; Li, D.; Abe, R., What is Degussa (Evonik) P25? Crystalline Composition Analysis, Reconstruction From Isolated Pure Particles and Photocatalytic Activity Test. *J. Photochem. Photobiol. A: Chemistry* **2010,** 216, 179-182.
27 Di Paola, A.; Cufalo, G.; Addamo, M.; Bellardita, M.; Campostrini, R.; Ischia, M.; Ceccato, R.; Palmisano, L. Photocatalytic Activity of Nanocrystalline TiO_2 (Brookite, Rutile and Brookite-based) Powders Prepared by Thermohydrolysis of $TiCl_4$ in Aqueous Chloride Solutions. *Colloid Surface A:* **2008**, 317, 366–376.
28 Di Paola, A.; Bellardita, M.; Marci, G.; Palmisano, L.; Parrino, F.; Amadelli, R. Preparation of Sm-loaded brookite TiO_2 photocatalysts. *Cat. Tod.* **2011**, 161, 35–40.
29 Stoll, S.; Schweiger, A. EasySpin, a comprehensive software package for spectral simulation and analysis in EPR *J. Magn. Reson.* **2006**, *178*, 42-55.
30 Lutterotti, L.; Matthies, S.; Wenk, H–R.; Schulz, A.J.; Richardon, J. Combined Texture and Structure Analysis of Deformed Limestone from Time-of-Flight Neutron Diffraction Spectra. *J. Appl. Phys.* **1997**, 81, 594-600. MAUD is available at http://www.ing.unitn.it/~maud.
31 Czoska, A.; Livraghi, S.; Chiesa, M.; Giamello, E.; Agnoli, S.; Granozzi, G.; Finazzi, E.; Di Valentin, C.; Pacchioni, G. The Nature of Defects in Fluorine-Doped TiO_2. J. Phys. Chem. C 2008, 112, 8951−8956.
32 Biedrzycki, J.; Livraghi, S.; Giamello, E,; Agnoli, S.; Granozzi, G. Fluorine- and Niobium-Doped TiO_2: Chemical and Spectroscopic Properties of Polycrystalline n‑Type-Doped Anatase. *J. Phys. Chem. C* **2014**, 118, 8462−8473.
33 P Chester, P. Cross-Doping Agent for Rutile Masers. *J. Appl. Phys.* **1961**, 32, 866−868.
34 Zimmermann, P. H. Temperature Dependence of the EPR Spectra of Niobium-Doped TiO_2. *Phys. Rev. B* **1973**, 8, 3917−3927.
35 Hasiguti, R. R. The Structure of Defects in Solids. *Ann. Rev. Mater. Sci.* **1972**, 2, 69-92.
36 Hajimoto, E.; Yamaka, E.; Nagasawa, M.; Shionoya, S. Electron Spin Resonance in Reduced SnO_2. *Phys. Lett.* **1966**, 23, 50-51.
37 Livraghi, S.; Maurelli, S.; Paganini, M. C.; Chiesa, M.; Giamello, E. Probing the Local Environment of Ti^{3+} Ions in TiO_2 (Rutile) by 17O HYSCORE. *Angew. Chem. Int. Ed.* **2011**, 50, 8038−8040.
38 Berger, T.; Diwald, O.; Knoezinger, E.; Napoli, F.; Chiesa, M.; Giamello, E. Hydrogen Activation at TiO_2 Anatase Nanoparticles. *Chem. Phys.* **2007**, 339, 138−145.
39 Akihiro Furube, Tsuyoshi Asahi, Hiroshi Masuhara, Hiromi Yamashita, Masakazu Anpo, Charge carrier dynamics of standard TiO_2 catalysts revealed by femtosecond diffuse reflectance spectroscopy. *J. Phys. Chem. B* **1999**, 103, 3120-3127.
40 Howe, R. F.; Gratzel M. EPR Observation of Trapped Electrons in Colloidal TiO_2. *J. Phys. Chem.* **1985**,n89, 4495-4499.
41 Morterra, C. An Infrared Spectroscopic Study of Anatase Properties. *J. Chem. Soc.***,** *Faraday Trans. I* **1988**, 84**,** 1617-1637.
42 Brant, A. T.; Gilles, N. C.; Yang, S.; Sarker, M. A. R.; Watauki, S.; Nagao, M.; Tanaka, I.; Tryk, D. A.; Manivannan, A.; Halliburton, L. E. Ground State of the Singly Ionized Oxygen Vacancy in Rutile TiO_2. *J. Appl. Phys.* **2013**, 114, 113602.
43 Chiesa, M.; Paganini, M. C.; Livraghi, S.; Giamello, E. Charge Trapping in TiO_2 Polymorphs As Seen by Electron Paramagnetic Resonance Spectroscopy. *Phys. Chem. Chem. Phys.* **2013**, 15, 9435−9447.
44 Meagher, E. P.; Lager, G. A.; Polyhedral Thermal Expansion in the TiO_2 polymorphs: refinement of the crystal structuresof rutile and brookite at high temperature. *Canadian Mineral.* **1979**, 17, 77-85.
45 M. Horn, C. F. Schwerdtfeger Refinement of the structure of anatase at several temperatures. *Zeitschrift fur Kristallographie* **1972**, 136, 273-281.
46 S. Maurelli; S. Livraghi; M. Chiesa; E. Giamello; S. Van Doorslaer; C. Di Valentin; G. Pacchioni Hydration Structure of the Ti(III) Cation as Revealed by Pulse EPR and DFT Studies: New Insights into a Textbook Case. *Inorg. Chem.* **2011**, 50, 2385-2394.